Pure Appl. Chem., Vol. 82, No. 4, pp. 931–951, 2010.
doi:10.1351/PAC-CON-09-11-36

Chemomechanics with molecular force probes*

Zhen Huang and Roman Boulatov‡

Department of Chemistry, University of Illinois, Urbana, IL 61801, USA

Abstract: Chemomechanics is an emerging area at the interface of chemistry, materials science, physics, and biology that aims at quantitative understanding of reaction dynamics in multiscale phenomena. These are characterized by correlated directional motion at multiple length scales—from molecular to macroscopic. Examples include reactions in stressed materials, in shear flows, and at propagating interfaces, the operation of motor proteins, ion pumps, and actuating polymers, and mechanosensing. To explain the up to 10^{15}-fold variations in reaction rates in multiscale phenomena—which are incompatible within the standard models of chemical kinetics—chemomechanics relies on the concept of molecular restoring force. Molecular force probes are inert molecules that allow incremental variations in restoring forces of diverse reactive moieties over hundreds of piconewtons (pN). Extending beyond the classical studies of reactions of strained molecules, molecular force probes enable experimental explorations of how reaction rates and restoring forces are related. In this review, we will describe the utility of one such probe—stiff stilbene. Various reactive moieties were incorporated in inert linkers that constrained stiff stilbene to highly strained macrocycles. Such series provided the first direct experimental validation of the most popular chemomechanical model, demonstrated its predictive capabilities, and illustrated the diversity of relationships between reaction rates and forces.

Keywords: electrocyclic reactions; force spectroscopy; molecular strain; nucleophilic displacement; photoisomerization; reaction dynamics; stressed materials; transition states.

INTRODUCTION

The vast majority of chemical reactions that comprise chemistry can be understood by considering the motion of a fairly small number of atoms, i.e., these reactions occur at a single (molecular) length scale. In contrast, in multiscale phenomena the nuclear motion that converts a reactant into the product(s) is coupled dynamically to a directional motion of a micro-, meso-, or macroscopic object (i.e., at scales >50 nm) [1–5]. Such coupling affects the rate at which the chemical reaction occurs and therefore must be accounted for in any kinetic model of such reactions. The common strategy to do so is to include a quantifier of such coupling as an explicit kinetically significant variable in the standard kinetic theories of Eyring or Kramers [6,7].

One of the simplest examples of a multiscale phenomenon in chemistry is the operation of an internal combustion engine, during which the macroscopic motion of the piston is driven directly by oxidation of C–H and C–C bonds. Whereas the rate of this macroscopic motion is governed by the rate of the chemical reaction, its direction is determined solely by the engine geometry rather than by how atoms move during the reaction. Such nondirectional (or scalar) dynamic coupling across scales is

Pure Appl. Chem. **82**, 757–1063 (2010). An issue of reviews and research papers based on lectures presented at the 13th International Symposium on Novel Aromatic Compounds (ISNA-13), 19-24 July 2009, Luxembourg City, Luxembourg on the theme of aromaticity.
‡Corresponding author

quantified by pressure, and its effect on the reaction rate is governed by the reaction's volume of activation, $\Delta V^{\ddagger}$ [8]. Other examples of scalar dynamic coupling across multiple length scales are the operation of certain actuating polymers (e.g., swell-gels), where changes in volume in response to a bulk chemical reaction (such as protonation/deprotonation) are used to drive directional macroscale motion [9].

The situation is much more interesting—and more complex—when the coupling is also directional, i.e., when the nuclear motion that constitutes a chemical reaction is correlated both spatially and temporally with those of the coupled microscopic object [1,6,10]. This so-called chemomechanical coupling is pervasive in nature. Examples include reactions in shear flows [7], formation and propagation of cracks in materials, fragmentation of macromolecules at interfaces [11], the operation of motor proteins (such as myosin and kinesin) [4], and certain molecular pumps, and mechanosensing [12]. It has also been realized in synthetic systems, including various single-molecule force experiments [13], certain small-molecule "motors" [2,3], and anisotropically aligned actuating polymers [14].

The directionality of multiscale coupling in these processes profoundly affects the dynamics of the chemical reaction. For example, interactions between rapidly flowing solvent and a dissolved macromolecule can accelerate dissociations of its backbone C–C bonds up to 10^{15}-fold, resulting in rapid macromolecular fragmentation [6,7]. However, the magnitude of the kinetic perturbation depends strongly on the relative orientation of the scissile bond and the axis of macroscopic motion (in this case, solvent flow). This strong orientational dependence of the rate cannot be accommodated within the standard models of chemical kinetics and requires that the perturbation be described by a vector (see below). Chemomechanics—an emerging field that aims at quantitative understanding of reaction dynamics in multiscale phenomena—is built on using force as such a vector.

An important class of chemomechanical phenomena involves localized chemical reactions in which just a few covalent bonds within a small reactive moiety (<1 nm) rearrange. Examples (Fig. 1) include homolytic and heterolytic cleavage of covalent bonds (A–D) [4,11,15,16] and isomerizations (E) [2]. Yet, compared to the extensively studied strain-induced dissociations of weak interactions (e.g., disruption of hydrogen bonding in forced unfolding of biopolymers) [17,18], chemomechanical processes arising from localized reactions have been little studied. Because of their small number of rearranging bonds and simple mechanisms, localized reactions comprise the most conceptually tractable systems for revealing fundamental insights into chemomechanical coupling. Covalent bond rearrangements involve large energy changes, making them particularly attractive as the basis of novel functional materials and processes for molecular-level control of energy transductions across length scales. Examples include self-assessing, self-healing, and actuating polymers [1,15,19,20], catalysts activated by bulk stresses [16], and autonomous nanomechanical devices propelled by structural rearrangements in reacting molecules (Fig. 1) [2,3,21,22].

This review focuses on chemomechanics of such localized reactions. First, we introduce a general framework—based on the concept of molecular restoring force—for understanding kinetics of such reactions. Second, we present an integrated experimental/computational approach that we developed for testing this framework. Third, we illustrate its utility with two simple chemical reactions: C–C and S–S bond dissociations. We do not discuss conformational changes of macromolecules caused by strain-induced dissociations of weak interactions, which dominate, for example, forced unfolding of proteins and nucleic acids, induced chain slippage, macromolecular desorption, and similar rearrangements at the supramolecular level. These phenomena have been extensively reviewed in the past [1,13,18,23]. Also, outside the scope of this review are synthetic "molecular motors" where analysis of conformational changes may not benefit from the chemomechanical formalism or reveal insights in the coupling between localized reaction dynamics and bulk stresses [24].

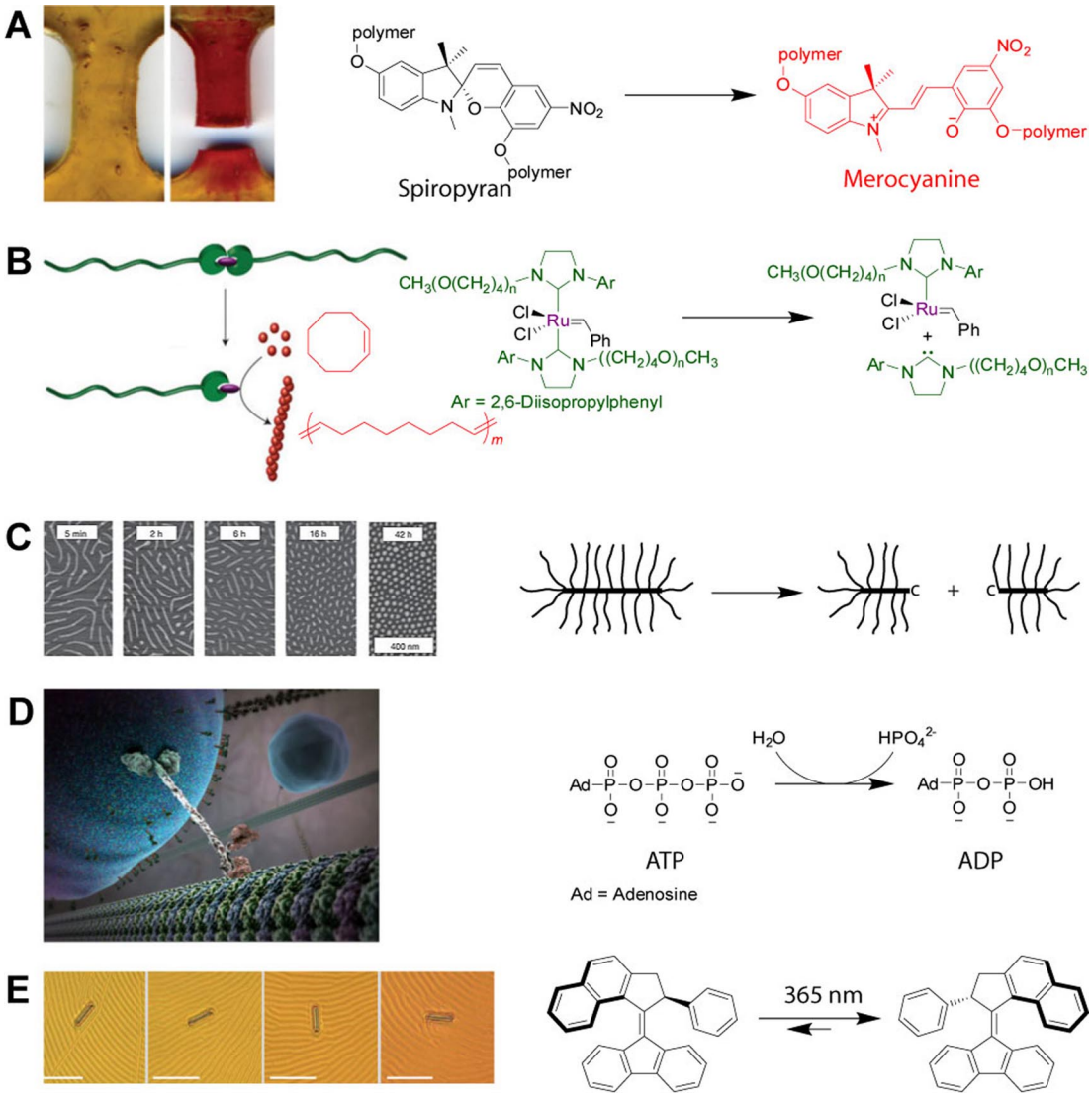

Fig. 1 Examples of chemomechanical phenomena involving localized reactions. (A) Stretching a polymer containing spiropyran leads to a color change presumably due to stabilization of the colored isomer by bulk stress that develops when the material is distorted. This stress-induced coloration may enable autonomous damage-sensing materials in which color changes would reveal locations of highest internal stresses where the material is most likely to fail [15]. (B) A shear-flow-induced dissociation of a polymer containing a Ru-biscarbene complex produces an active catalyst for ring-opening metathesis polymerization [16]. (C) Absorption of brush-like polymers on liquid/solid interface results in multiple C–C bond scission events, which are accelerated by tensile forces along the backbone [11]. (D) Kinesins "walk" along microtubule tracks to transport microscopic objects thousands times larger than themselves by transducing and amplifying small-magnitude nuclear motion during nucleopilic dissociation of the P–O bond of adenosine triphosphate (ATP) [4]. (E) Irradiation of a liquid-crystalline film incorporating a chiral aromatic olefin results in unidirectional rotation of a microscopic object driven by photoisomerization of the central C=C bond. Only the first step of the proposed photo- and thermochemical four-step cycle is shown. Molecular actuation based on the *Z*/*E* photoisomerization holds promise for powering the propulsion of autonomous nanomechanical devices [2].

CHEMOMECHANICAL KINETIC MODEL

Quantitative understanding of dynamic multiscale coupling holds great potential to establish both a truly molecular picture of the response of materials to mechanical loads and a conceptual framework to guide the design of new materials capable of much more complex responses to such loads than is currently possible [1]. Realization of this potential requires a general, quantitative, and predictive model to relate bulk stresses to molecular reaction rates. In chemomechanics, such a model uses force to quantify energy coupling across length scales [25–28]. It offers a strategy to simplify the complex question of reaction dynamics in multiscale phenomena by breaking it down into two simpler questions: (1) How are forces at different length scales related, from the macroscopic force that accounts for large-scale distortion in material in response to an external load down to molecular forces that quantify geometrical perturbations of individual molecules? (2) How do reaction rates depend on the molecular restoring force of the reactant(s)?

Much progress has been made in answering question 1 [29]. The second question, however, remains far less understood. One approach to solving it has been to incorporate force into the standard models of chemical kinetics. Such models, however, are based only on scalar variables, such as temperature (Arrhenius and Eyring theories), pressure, viscosity (Kramers theory), and dielectric constant (Marcus theory), and extending them to vectoral variables poses unique challenges that remain unresolved.

Strain energy: An extensive scalar measure of molecular strain

Qualitatively, dramatic changes in reaction rates in chemomechanical phenomena could be understood as a manifestation of molecular strain [30,31]. Unlike macroscopic strain, molecular strain is a qualitative concept. Molecular strain has traditionally been quantified as strain energy, defined as the difference in the free energy of a strained molecule and the (often hypothetical) strain-free analog. Although strain often raises the energy of both the ground and transition states, a thermal reaction of a strained reactant that allows (partial) relief of the ground-state strain in its transition state would be accelerated. Its activation free energy would be decreased by the amount of the relieved strain energy compared with the activation free energy of the strain-free analog. Although it is rarely possible to accurately estimate this amount without the detailed knowledge of the transition-state geometry (which would negate the value of the concept of strain for chemical kinetics), the model has been remarkably useful in guiding chemical thinking for over a century [30,32].

Strain energy, however, fails to account quantitatively for the observed changes in reaction rates resulting from correlated motion across length scales and thus cannot form the basis of chemomechanics. Energy is an extensive (size-dependent) property. Its application to reactions of small molecules, with their well-defined molecular sizes, is straightforward. In chemomechanical phenomena, which occur at the interface where the atomistic and continuum behaviors of matter meet, identifying the area or volume over which the kinetically significant strain energy is distributed has been impossible. Furthermore, energy is a directionless (scalar) parameter, which fails to capture the directional nature of kinetically significant molecular strain (i.e., the direction in which the reactive moiety is distorted matters in how fast the molecule reacts). For example, fragmentation rates of stretched macromolecules do not correlate with their total ground-state strain energies, or strain energy per chemical bond, even in such chemically homogeneous polymers as polysiloxanes, whose backbones are comprised exclusively of identical Si–O bonds [33].

Restoring force: An intensive vectoral measure of molecular strain

An alternative quantifier of kinetically significant strain is molecular restoring force, defined as the gradient of strain energy along a molecular axis [28]. Force is a scale-free (intensive) property: any object,

from molecular to macroscopic, develops restoring force when distorted from its optimal geometry. An example of macroscopic restoring force is the force that develops when a rubber band is stretched.

Molecular restoring force is a vectoral intensive measure of strain [28,31,34]. One can therefore expect that a rate/force relationship is an intrinsic property of a chemical reaction, independent of both the size of the molecule within which the reaction occurs and the process which strains the molecule. In other words, a reactive moiety distorted to the same restoring force will react at approximately the same rate regardless of the total size of the molecule.

Quantitative models relating rate and restoring force

Although multiple relationships between reaction rates and restoring forces of strained reactants have been proposed [17,35–38], no fundamental laws are known that would dictate any particular form of such a relationship [28]. Under such circumstances, the most systematic approach to quantitative analysis of chemomechanical kinetics may be to represent the ensemble-averaged rate constant k_f for a reactant distorted to restoring force f as a Taylor expansion around the rate constant of the strain-free reaction, k_0. Equation 1 is written in a coordinate system defined by the force vector (i.e., $f_z = f, f_x = f_y = 0$) and is valid for both time-invariant and -dependent force.

$$\underbrace{\ln k_f = \ln k_0 + f\frac{\partial \ln k}{\partial f}}_{1^{st}\text{-order Taylor expansion}} + \frac{1}{2}f^2\frac{\partial^2 \ln k}{\partial f^2} + \ldots \quad \underbrace{\qquad\qquad}_{2^{nd}\text{-order Taylor expansion}} \tag{1}$$

Truncating eq. 1 at the linear (1st-order) term and expressing k_0 in the formalism of the transition-state theory yields the most commonly used chemomechanical model (eq. 2) [6,17]. In this model, $\Delta x = k_B T \frac{\partial \ln k}{\partial f}$ is often interpreted as the difference, along the force vector, in the "length" of the reactant between its ground- and transition-state geometries, but it is best viewed as an empirical parameter which may or may not have a geometrical interpretation [39].

$$k_f = \frac{k_B T}{h} e^{-\left(\Delta G^{\ddagger} - f\Delta x\right)/k_B T} \tag{2}$$

Equation 2 is often referred to as the standard chemomechanical model, first proposed by Eyring in the 1940s [7] and later elaborated upon by Bell and Evans, who also derived it from the Kramers theory of reaction kinetics [18,40,41]. A graphical representation of eqs. 1–2 is a modified 1D free energy profile of the reaction in the presence of force (Fig. 2).

Equation 2 is based on a number of assumptions whose validity remains to be established [17]. For it to be predictive, the value of Δx must be derivable from the strain-free molecular geometries of the reactant (and possibly the transition state), i.e., it must have a well-defined molecular interpretation.

CONVENTIONAL FORCE SPECTROSCOPY WITH MICROSCOPIC FORCE PROBES

The development of the chemomechanical formalism requires a general and accurate method to measure kinetics and mechanisms of diverse reactions as a function of the restoring force. Micromanipulation techniques [13], including atomic force microscopy (AFM) and optical tweezers, allow the total restoring force of a single long macromolecule (or a series of macromolecules connected

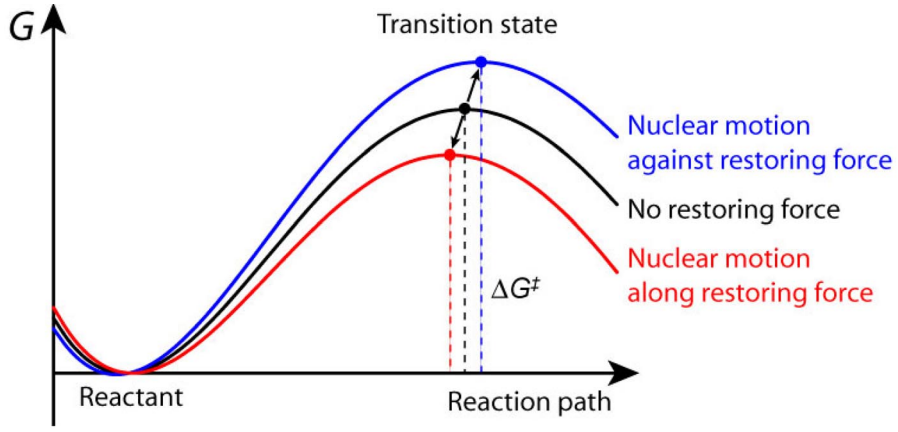

Fig. 2 The standard chemomechanical model (eq. 2) postulates that the original free energy profile (center curve) along the reaction path changes in the presence of restoring force proportionally to its magnitude [6,17]. The barrier decreases when the net motion of atoms that converts the reactant into the transition states occurs along the force vector (bottom curve). Otherwise, the barrier increases (top curve). The Hammond postulate requires that the transition-state geometry changes in conjunction with the energetic changes in the transition state relative to the reactant and product: a barrier-lowering perturbation shifts the reactant and transition state toward a common geometry, whereas a barrier-raising perturbation shifts the transition state toward the product geometry. Such force-dependent geometrical changes would be quantified by the 2nd-order (quadratic) Taylor coefficients in eq. 1 but are neglected in the standard Bell–Evans models (e.g., eq. 2) [18,40,41].

in a daisy chain) to be controlled.* In these single-molecule force experiments a macromolecule is connected at its termini to a pair of microscopic force probes, which are then separated at a desired rate (or until a desired restoring force is reached), stretching the macromolecule (Fig. 3). The resulting deflection of the force probe from its equilibrium position (bead in the optical tweezers) or equilibrium geometry (AFM tip) is measured and is converted into restoring force with the help of empirical calibration curves.

The micromanipulation approach is predicated on the force probe and the attached macromolecule being in mechanical equilibrium, which may or may not occur experimentally. This need of the internal mechanical equilibrium makes single-molecule force spectroscopy (SMFS) a fairly slow technique. It takes milliseconds for the microscopic force probe to adopt an equilibrium geometry after the restoring force of the attached macromolecule has changed, for example, because it underwent a chemical reaction. In contrast, chemical reactions occur on time scales ranging from picoseconds for localized covalent bond rearrangements to microseconds for changes in global macromolecular conformations. Consequently, SMFS measures the contour length of the attached macromolecule averaged over >1 ms. The unique capability of SMFS is to monitor large-scale (>1 nm) conformational changes such as those during biopolymer unfolding. This capability has, over past two decades, revolutionized our understanding of the mechanical properties of proteins, nucleic acids, and synthetic macromolecules, and provided important insights into the energy landscape of their conformational changes [13,17,18].

Far fewer attempts to apply the SMFS methodology to study chemomechanics of localized reactions have been reported. In a representative example, Craig et al. studied the nucleophilic dissociation of a Pd–N bond in a polymer whose restoring force was gradually increased and demonstrated a linear

*Macromolecules can also be stretched in elongational or turbulent flows that are generated, for example, by sonication of a polymer solution [15,19,42]. In these experiments, however, the resultant changes in molecular geometry or the restoring forces cannot yet be quantified.

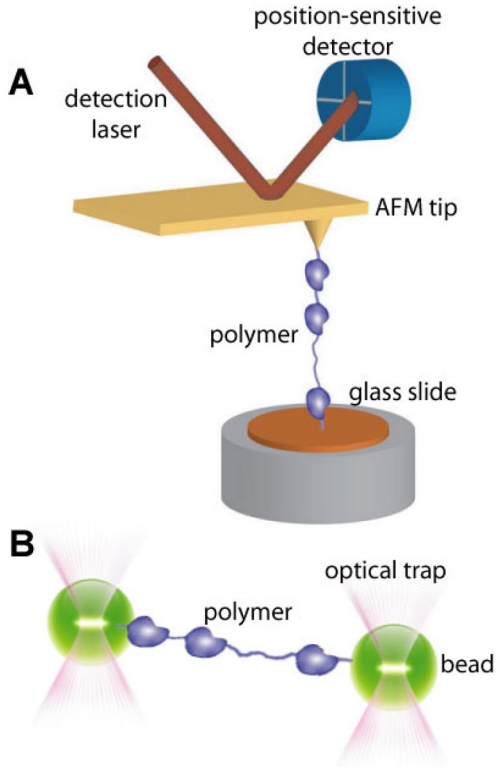

Fig. 3 Conventional force spectroscopy based on (A) AFM or (B) optical tweezers [13].

dependence between $\ln k_f$ and the total restoring force at the time of fragmentation [43]. Fernandez et al. measured the kinetics of nucleophilic scissions of the S–S bonds in engineered oligoproteins maintained at a constant average restoring force and observed two different linear dependences of $\ln k_f$ vs. total force, one below ~500 pN and another above [44]. In either case, the observed Δx values (in eq. 2) remain to be interpreted molecularly and their proposed structural interpretations to be validated. Because SMFS only reports the contour length of the macromolecule, localized reactions resulting in macromolecular fragmentation are most amenable to such studies, since structural changes due to other types of chemical reactions are less than the magnitude of thermal fluctuations of the macromolecule [13]. An alternative approach has used polymers containing a large number of equivalent reactive moieties, as exemplified by single-molecule force experiments on oligoazobenzenes [14]. Upon irradiation of a predominantly *E*-isomer, a fraction of the azobenzene monomers underwent the $E \rightarrow Z$ photoisomerization, generating shorter *Z*-monomers and a concomitant contraction of the polymer against the restoring force of the distorted AFM tip. However, the complexity of this system has so far precluded a quantitative molecular interpretation of the results [45].

Despite the ever-expanding applications of conventional force spectroscopy, systematic studies of force-dependent kinetics of localized reactions remain outside of its reach. Both the surface roughness of microscopic force probes and thermal fluctuations of long macromolecules exceed the dimensional change resulting from many localized reactions, making them essentially invisible to the technique [13]. The restoring force of the reactive moiety is also difficult to quantify because its orientation relative to the pulling axis of the macromolecule is rarely if ever known. The uncertainty about the internal mechanical equilibrium in such experiments and conformational heterogeneity of the polymers even at fairly high strains further complicates interpretations. More importantly, in such experiments the kinetics of localized reaction may be governed by molecular degrees of freedom that are far removed from

the reaction moiety due to complex tertiary structures of polymers. Because such degrees of freedom are much softer than the highly localized coordinates (bond distances, bond angles, and torsions) of the reactive moiety, they may dominate the observed force-rate correlations [1]. For example, strain-dependent tertiary structure of oligoproteins studied to date may affect bimolecular kinetics by altering mass transport to the reactive site rather than the site's intrinsic reactivity [39]. Further complicating such studies are the narrow dynamic range (0.01–100 s) [13], intrinsically limited statistics [46], inaccessibility of product characterization, and challenges of variable-temperature single-molecule force measurements, as well as the complex analysis needed to account for nonequilibrium strain distributions.

A MOLECULAR FORCE PROBE: STIFF STILBENE

Hence, systematic studies of chemomechanical kinetics of localized reactions require a complementary strategy. We have developed one such strategy, which relies on molecular design instead of micromanipulation techniques to control the restoring force of diverse reactive moieties up to 600 pN in <30 pN increments (Fig. 4) [25–27]. This approach utilizes a molecular force probe, an inert molecule whose restoring force is varied predictably by constraining a single nonbonding internuclear distance. Constraining this distance with an inert linker containing a reactive moiety creates in this moiety the restoring force equal in magnitude and opposite in direction to the force of the molecular force probe. A homologous series of macrocycles across which the reactive moiety experiences increasing restoring force is obtained by using linkers of different length and conformational flexibility. The macroscopic

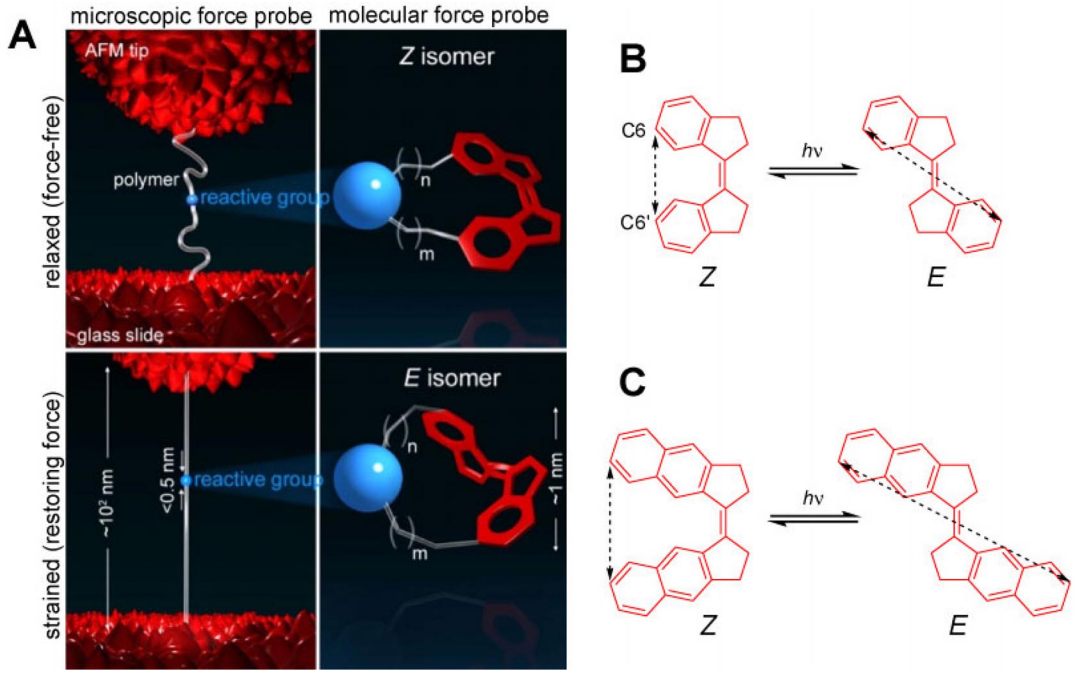

Fig. 4 (A) A schematic comparison of force spectroscopy of localized chemical reactions with an AFM that uses a microscopic force probe (left) and with a molecular analog based on stiff stilbene (right) [26]. The comparable sizes of the molecular force probe and the reactive moiety greatly facilitate both the acquisition and interpretation of rate/force relationships of such reactions. The structures of *Z* and *E* stiff stilbene (B) and the next polyaromatic homologue, 1,1'-bis(benzindanylidene) (C), are shown. Notice the difference in the separation of a pair of C atoms in the two isomers (the broken arrows).

analog of this molecular architecture is a semi-rigid rod whose ends are tied by a rope shorter than the rod itself. The bent rod exerts purely tensile force on the rope and anything in the rope. The longer the rope, the smaller the distortion of the rod and hence the restoring force of the rope.

To be broadly useful for studying chemomechanics of localized reactions, a molecular force probe should have [25,26]: (1) a size that is small enough to allow high-level quantum-chemical calculations of geometries and energies of kinetically relevant structures yet large enough compared to the reactive moieties to dominate the fraction of the ground-state strain energy that account for changes in the barrier height; (2) high structural anisotropy to localize its strain into the constrained internuclear distance along which the force probe is coupled to the reactive moiety; (3) high chemical inertness under conditions used for measuring the chemomechanical kinetics of the substrate reaction; and (4) easily accessible highly strained conformations.

Whereas the number of suitable molecular force probes will undoubtedly increase as this approach is adopted broadly, we have been exploiting molecular force probes based on pairs of *Z* and *E* geometrical isomers of alkenes [25–27] and their analogs (e.g., azobenzenes). Because photoisomerization of C=C or N=N bonds offers ready access to highly strained geometries, these compounds have been explored as molecular switches and unidirectional rotors (e.g., Fig. 1E) [2,3], and building blocks for photoactuating and photoswitching materials [14,47].

While the most popular members of this family of compounds, stilbene, tetrabenzafulvalene, and azobenzenes, are too conformationally flexible to be useful molecular probes, stiff stilbene (1,1'-biindanylidene **1**, Fig. 4B) meets the criteria of a general force probe [25–27]. Like the better known stilbene (1,2-diphenylethylene), stiff stilbene exists in two isomers, *Z* and *E*, which are separated by a high barrier for thermal isomerization (~43 kcal/mol*), but interconvert readily in highly efficient photoisomerization at 360–400 nm. Both C6···C6' and C5···C5' distances undergo large change upon isomerization of stiff stilbene and are by far the softest degrees of freedom in stiff stilbene. Constraining either distance with a linker that is longer than the equilibrium value in the *Z*-isomer but is shorter than that in the *E*-analog yields 15–20 atom macrocycles, which are strain-free when containing *Z* stiff stilbene but increasingly strained in the *E* form.

Restoring forces of reactive moieties that contribute up to 6 atoms to the size of the macrocycle can be varied over ~600 pN in 30–50 pN increments by changing the chemical composition of the chains connecting the reactive moiety to stiff stilbene. The molecular size of the vast majority of functional groups in chemistry is suitable to yield the required macrocyclic series. This method can be extended to even larger reactive moieties by replacing stiff stilbene with its polyaromatic homologs, such as 1,1'-bis(benzindanylidene) (Fig. 4C).

Strain-free *Z*-macrocycles are readily accessible by intramolecular McMurry coupling, which is a general, high-yielding, and straightforward protocol to assemble regio- and chemoselectively C=C bonds [49]. Irradiation with ~400 nm light converts these *Z*-macrocycles to the *E*-isomers with up to 28 kcal/mol of strain energy. Accessing such highly strained molecules by any other synthetic protocol would in general be quite challenging. Since many functional groups of interest to organic, inorganic, and materials chemists are transparent in the 360–400 nm window, reliance on photoisomerization to generate restoring forces does not significantly narrow the range of reactive groups that can be studied by this method. This is complemented by the relative inertness of stiff stilbene to allow systematic studies of diverse reactions, including electrocyclic reactions, nucleophilic substitutions, and eliminations. Finally, the high barrier of thermal *E*/*Z*-isomerization of parent stiff stilbene ensures that relaxation of even highly strained *E*-macrocycles to *Z*-isomers is often negligibly slow.

By eliminating microscopic force probes and macromolecular linkers, the molecular force probe offers important advantages for understanding chemomechanics [25–27]. The comparable size of the

*Compare this energy to the 23 kcal/mol activation free energy for *E*/*Z*-isomerization of azobenzene [14] and 35–20 kcal/mol barriers of tetrabenzofulvalene derivatives [48].

molecular force probe and the reactive moiety allows force spectroscopy on reactions in which the reactant and the product geometries differ by <1 Å. The small size of the macrocycles makes them amenable to high-level quantum-chemical calculations, which yield restoring forces without the ambiguities intrinsic to conventional force spectroscopy (see above), as well as geometrical parameters of the transition states (including all thermally accessible conformers). This modest size also allows mechanistic and kinetic interrogations by the whole arsenal of modern spectroscopic methods. Since all measurements are done on molecular ensembles rather than single molecules, extrapolation of thermodynamic values from limited-statistic measurements becomes unnecessary. Finally, analysis of the observed rate/force correlations is simplified by a comparatively small number of molecular degrees of freedom that control the reaction dynamics.

FORCE SPECTROSCOPY WITH MOLECULAR FORCE PROBES

A molecular force probe allows chemomechanics of diverse localized reactions to be measured and interpreted structurally and mechanistically by integrating molecular design, synthesis, kinetic/mechanistic studies and quantum-chemical computations following the steps described below.

Synthesis

Chemomechanical studies of each reaction require a series of 5–10 macrocycles of systematically varying size. The utility of this method is maximized when diverse series of such macrocycles are accessible using the same simple, high-yielding synthetic protocol. Such a protocol requires an efficient macrocyclization method compatible with diverse functional groups and linker compositions. Intramolecular McMurry coupling of a pair of ketones with a Ti/Zn reagent to yield a C=C bond [49] fits the bill, making diverse macrocyclic series accessible from four readily available substituted indanones (**2–5**, Fig. 5) in 2–5 steps and up to 75 % overall yields. To gain further synthetic flexibility, we have developed two variations of the overall protocol. In one, a pair of indanones connected by a 7–12 atom linker, which contains the reactive moiety of interest, is coupled to yield the desired *Z*-macrocycles. In the other version, such macrocycles are obtained by "plugging" reactive moieties into various 6,6'-disubstituted *Z* stiff stilbene diols (**6**). These diols are obtained on multigram scale by McMurry coupling of indanones bridged by sacrificial linkers that are too short for the formation of the *E* stiff stilbene core. The linker

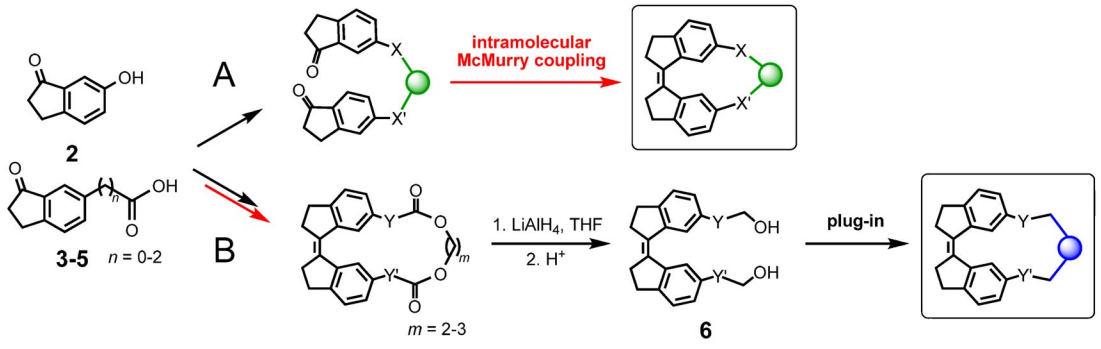

Fig. 5 Diverse series of macrocycles (rightmost structures) are synthetically accessible from four indanones (**2–5**) by one of the two routes [25–27,53]: (A) intramolecular McMurry coupling of a pair of indanones bridged by a linker containing the reactive moiety (green), and (B) reaction of various stiff stilbene diols (**6**) with suitable precursors of the reactive moiety (blue). Intramolecular McMurry coupling is shown in red arrows. Various chemistries can be used to plug in reactive moieties. Figure 6 illustrates a few representative linkers (X, X', Y, Y') we have used.

is removed by reduction. In both cases, asymmetrical macrocycles are as easily accessible as symmetrical ones. Irradiation of solutions of *Z*-isomers yields photostationary states containing up to 80 % of the *E*-isomers.

Kinetics

To eliminate the contribution of linkers to the rate variation across a series of macrocycles, we measure the kinetics of the substrate reaction in both isomers and analyze the differences, $\Delta\Delta H^{\ddagger} = \Delta H^{\ddagger}_{Z} - \Delta H^{\ddagger}_{E}$ and $\ln(k_E/k_Z)$, with the latter equivalent to $\ln(k_f/k_0)$ in eq. 1. The values of $\Delta\Delta H^{\ddagger}$ and $\ln(k_E/k_Z)$ of the highest accuracy are available from competition experiments using the photostationary states from irradiation of the *Z*-isomers. Hence, kinetic studies do not require isolation of the *E*-isomers. We have developed two methods to obtain such data depending on whether the substrate reaction is unimolecular [26] or bimolecular [27]. In rare cases when strained *E* stiff stilbene thermally relaxes to the strain-free *Z*-analog at a rate comparable to the conversion of the reactive moiety, extracting correct k_E and k_Z values requires the knowledge of the kinetics of *E*/*Z*-isomerization [25].

The progress of many reactions in the macrocycles can be conveniently monitored either by high-performance liquid chromatography (HPLC) or by changes in the electronic spectra of the reactive moiety or stiff stilbene. ^{1}H NMR spectroscopy is used to confirm the nature of the products. The rates in strain-free *Z*-macrocycles are often similar to those in non-macrocyclic reactants, suggesting that their incorporation into a macrocycle introduces little kinetic perturbation. The $\Delta H^{\ddagger}$ and $\Delta S^{\ddagger}$ values are obtained from rate constants measured over a 40–50 °C range.

The lifetimes of even the most strained *E*-isomers vastly exceed ~10 ps, which is the time it takes for stiff stilbene to dissipate excess thermal energy from the absorbed ~400 nm photon that induced photoisomerization. Therefore, in both *E*- and *Z*-isomers, the conversion of the reactive moieties to products is always a thermally activated process, making its kinetics independent of the mechanism by which the restoring forces have been generated. We use photoisomerization for its convenience, but any other process that creates the same restoring force in the reactive moiety would have an identical effect on the reaction rate.

Restoring forces

The modest size of the macrocycles allows their restoring forces to be obtained directly by quantum-chemical methods. The first step of such calculations is to establish that they correctly reproduce the measured $\Delta H^{\ddagger}$ and $\Delta G^{\ddagger}$ values for all isomers in a series. For all reactions studied so far, density functional theory (DFT) with H-GGA or HM-GGA functionals and triple-ζ quality basis sets has been sufficient to reproduce the measured energies with chemical accuracy (±1 kcal/mol). Solvent-dependent reactions (e.g., S_N2 substitutions, see below) are calculated with a continuum representation of the reaction solvent, usually within the conducting polarized continuum model (CPCM). Benchmarking of quantum-chemical calculations against experimental parameters is critical in establishing the validity of the calculated values that are inaccessible experimentally (including restoring forces and transition-state geometries). Our method remains unique among all experimental and theoretical studies of force-dependent rates to allow such benchmarking [1,37–39].

To reproduce the measured $\Delta H^{\ddagger}$ and $\Delta G^{\ddagger}$ values to within the acceptable accuracy, it is essential to identify the conformational global minimum for each kinetically significant structure. The knowledge of thermally accessible conformers also enables the calculations of ensemble-average structural differences between the ground and transition states and restoring forces. We identify such global minima by exhaustive conformational searches of each macrocycle first with molecular mechanics using a Monte Carlo algorithm, followed by reoptimization of a decreasing fraction of the lowest-energy conformers at increasingly higher levels of theory. The thermodynamic parameters are obtained within the statistical mechanics formalism in the ideal gas, harmonic oscillator, and rigid rotor approximations.

These thermodynamic parameters are compared against the experimental $\Delta H^{\ddagger}$ and $\Delta G^{\ddagger}$ values. When the acceptable level of agreement is achieved across the complete series, the corresponding structures are used to calculate the restoring forces at the same level of theory that reproduced measured activation parameters.

At a stationary point on its free-energy surface, a molecule is necessarily in internal mechanical equilibrium. In other words, the restoring forces of the strained reactive moiety and the molecular force probe in *E*-isomers exactly compensate each other, resulting in zero net force on the macrocycle. We have developed several strategies to reveal uncompensated restoring forces. Conceptually the simplest one is to quantum-chemically optimize a part of the macrocycle in which the reactive moiety is replaced with pairwise harmonic potentials between 1–2 atom pairs closest to the reactive moiety (Fig. 7A).

Because restoring force is independent of the nature of the constraint, both in the full macrocycle and in a fragment with pairwise potentials, the molecular force probe and the linkers adopt a geometry whose restoring force exactly compensates that of the constraint. During the quantum-chemical optimization of the fragment, the pairwise potentials are adjusted iteratively until two criteria are met: (1) the structure of stiff stilbene and the linkers reproduces that in the full macrocycle (as judged by the root-mean-square deviation of non-H atoms of the two moieties) and (2) each atom's total force, arising both from the molecular wavefunction and (for some atoms) the added pair-wise potentials, is zero.

The restoring force of the fragment in such converged structure is obtained simply based on the difference in separation of all atomic pairs for which potentials were defined from the zero-force separation defined for each potential. We prefer to optimize the probe-containing fragment rather than the reactive moiety, because the constrained axis of the probe (C6···C6') is much softer than that of the reactive moiety. This minimizes the errors in forces due to the difference between the geometries calculated with pairwise potentials and those in the corresponding macrocycles. Moreover, because the force probe is identical for all reactions, comparisons of the rate/force correlations of different reactions are fairly insensitive to any systematic errors or assumptions of the calculation procedure.

This procedure is repeated for all thermally accessible conformers of both isomers of each macrocycle in the series to obtain ensemble-averaged restoring forces. Small, but non-zero, restoring forces in *Z*-isomers may reflect an intrinsic accuracy of the force calculations. Regardless of the molecular origin of the non-zero restoring forces in *Z*-isomers, within the formalism of eq. 1, the vectoral difference of the restoring forces in the *E*-isomer and its *Z*-analog accounts for the ratio $\ln(k_E/k_Z)$.

This integrated experimental/computational approach yields the data needed to understand chemomechanics of localized reactions: (1) measured rate differences between the two isomers, (2) calculated differences in the restoring forces that account for the rate differences, and (3) the molecular structures of ground and transition states that govern how rates and forces are related. In the next section, we illustrate our methodology with two elementary (i.e., single-barrier) reactions: the homolytic scission of a C–C bond in cyclobutene [25,26] and nucleophilic scission of the S–S bond in a disulfide [27].

APPLICATIONS OF MOLECULAR FORCE PROBES: FORCE-DEPENDENT KINETICS OF THE C–C AND S–S BOND DISSOCIATIONS

A reaction uniquely suitable for quantitative evaluation of chemomechanical models is the concerted dissociation of the C–C bond during ring opening of cyclobutene and its derivatives (Fig. 6A). The kinetics and mechanism of this reaction are well established, as is its transition-state geometry, which has been calculated at many levels of theory [50]. Its kinetics is insensitive to solvent or substituents; and many derivates are easy to synthesize [50]. Consequently, the reaction has been the subject of several pioneering experimental and theoretical chemomechanical studies [19,37,38].

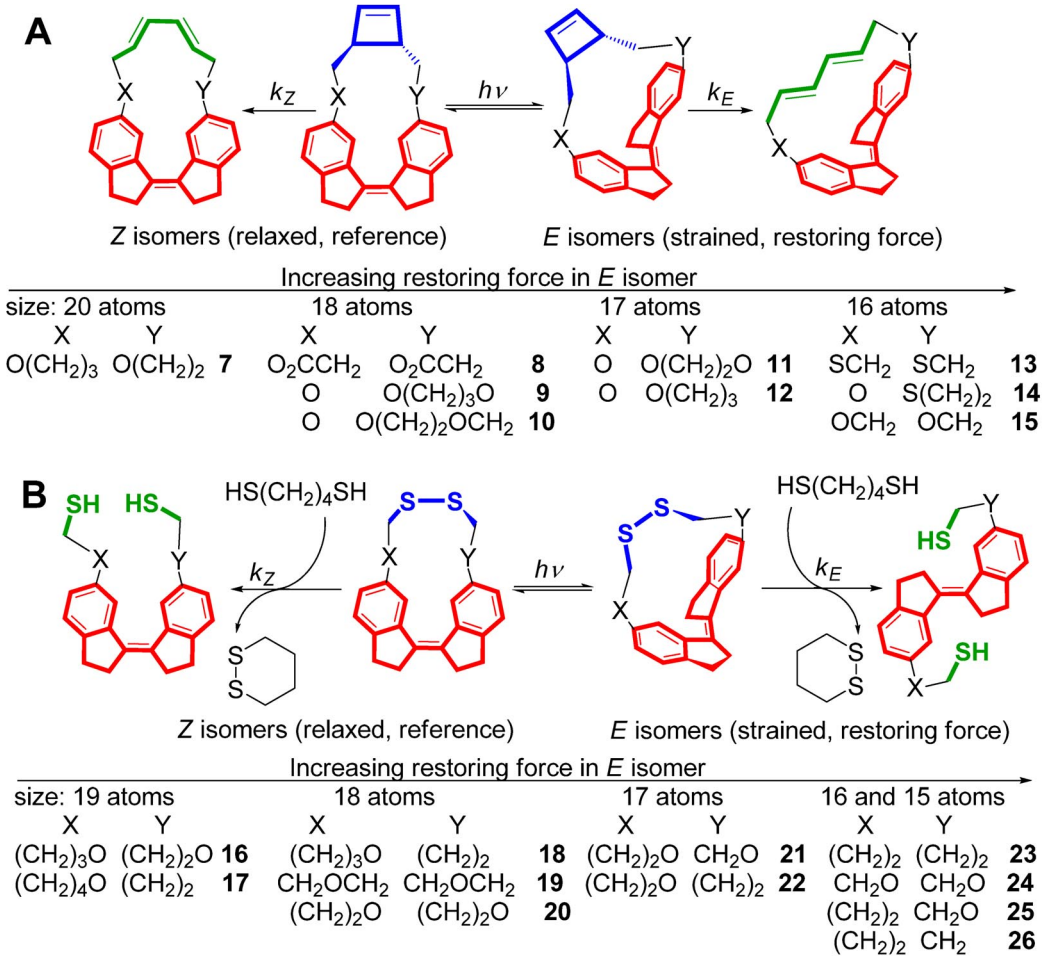

Fig. 6 Two series of stiff stilbene macrocycles containing (A) cyclobutene [25,26] or (B) the disulfide bond [27], and their reactions. Stiff stilbene is red, the reactive moieties are blue; the products of their reactions are green. In the definition of the linkers X and Y, the atom on the right is bound to stiff stilbene.

The force-dependent kinetics of thiol/disulfide exchange (Fig. 6B) has also attracted considerable interest, both from a fundamental physicochemical viewpoint and for its potential roles in biological mechanotransduction [51]. As shown by Whitesides et al. and others, the reaction proceeds through a classical S_N2 rate-determining step in which thiolate attacks one of the S atoms of the disulfide bond (Fig. 6B) [27,52]. The kinetics of thiol/disulfide exchange in stretched titin appears to increase rapidly with force up to ~500 pN, but is only weakly force-dependent at higher forces [44]. The originally proposed mechanism, which attributed the acceleration to increased intrinsic reactivity of the disulfide moiety due to elongation of the S–S bond from the ground to the transition states [53], was recently challenged [39], making thiol/disulfide exchange a reaction of particular interest for investigation by a molecular force probe.

Synthesis and kinetic measurements

The cyclobutene series **7–15** was synthesized in 3–11 steps and 2–34 % total yields following scheme A (Fig. 5) [25,26]. Because the S–S bond is incompatible with McMurry coupling, the disulfide-con-

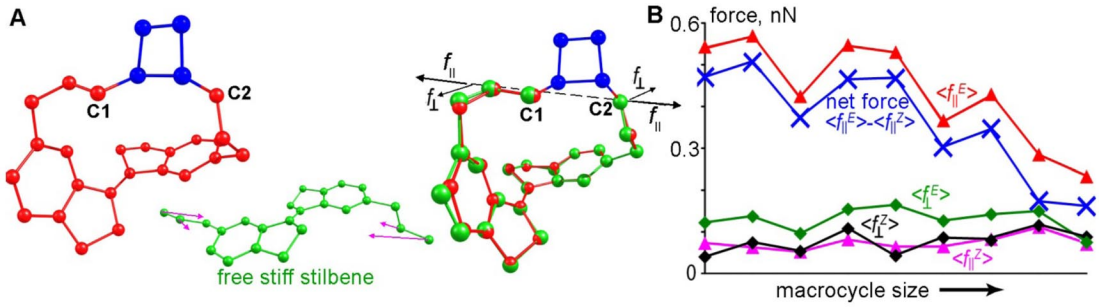

Fig. 7 Restoring forces of cyclobutene across a series of macrocycles **7–15** [26]. (A) A schematic illustration of the method for calculating the restoring forces on example of macrocycle **15**. The fragment of free stiff stilbene and linkers is quantum-mechanically optimized with pairwise harmonic potentials. The overlay shows that the structure of stiff stilbene and linkers reproduced that in the full macrocycle. (B) Ensemble-average restoring forces in macrocycles **7–15** projected on and orthogonal to the C1···C2 molecular axis. Representative of both series, the restoring forces in *E*-isomers are predominantly along the C1···C2 axis and correlate inversely with the macrocycle size. The forces are small in the strain-free *Z*-analogs.

taining macrocycles **16–26** were synthesized by the "plug-in" method B in 4–6 steps and >10 % overall yields [27,54]. Clean high-yielding macrocyclization was achieved by oxidation of thiols under high dilution.

The activation parameters for the two reactions were obtained by following the reaction progress by HPLC. The C–C bond homolysis of cyclobutene in *E*-macrocycles occurred up to 5×10^6-fold faster (at room temperature) compared to that in the *Z*-analogs. The acceleration was purely enthalpic with the $\Delta\Delta H^{\ddagger}$ values ranging from 1.7 ± 0.5 to 9.1 ± 0.9 kcal/mol across the 9-macrocycle series. In the *E*-isomers of the smallest macrocycles, **13–15**, ring opening of cyclobutene competed with thermal relaxation of the highly-strained *E* stiff stilbene, decreasing the lifetime of the *E*-macrocycles to <100 ms.

In contrast, the rate constants of thiol/disulfide exchange in the two isomers of any disulfide macrocycle was within a factor of 2, with the correspondingly small values of $\Delta\Delta H^{\ddagger}$ and $\Delta\Delta S^{\ddagger}$. Whereas rate constants of individual isomers manifested the expected strong solvent dependence, the ratios k_E/k_Z were solvent-independent. The activation parameters in the *E*-isomers of the smallest macrocycles (**23–26**) could only be obtained computationally, as irradiation of the *Z*-isomers of **23–26** resulted in homolysis of the S–S bond [54].

Computed restoring forces

All measured $\Delta H^{\ddagger}$ values for the C–C bond scission in cyclobutene were reproduced to within ±1 kcal/mol at the O3LYP/6-311G(2d,p) level of DFT. For thiol/disulfide exchange, B3LYP/6-311+G* in CPCM using united-atom solute cavities with standard (UFF) atomic sizes gave best agreement with the experiment. Computations using explicit solvation (1–2 water molecules) as well as CPCM with cavities using Hartree-Fock (HF)- or DFT-optimized atomic sizes gave worse agreement with the experiment.

Figure 7 illustrates the part of the cyclobutene-containing macrocycles used to calculate restoring forces and the calculated values in all nine macrocycles of the series. Since force is a vector, its orientation is as important as its magnitude. To convey the directionality of the calculated forces, they are presented as projections on and orthogonal to the molecular axis defined by the C1/C2 atoms of the reactive moiety. The calculated restoring forces in *Z*-macrocycles were <100 pN, not aligned with a particular molecular axis and uncorrelated with the macrocycle size ($f_{\parallel}^{Z}$ and $f_{\perp}^{Z}$ in Fig. 7B).

In contrast, the restoring forces in *E*-isomers were closely aligned with the C1···C2 axis ($f_{\parallel}^{E} > f_{\perp}^{E}$) and increased in smaller macrocycles, consistent with chemical intuition. The net force was obtained by subtracting the force calculated for *Z*-macrocycles from that in the *E*-analog. The restoring forces in the transition states of cyclobutene ring opening in *E*-macrocycles were ~90 % of those in the reactants, reflecting partial conformational relaxation of stiff stilbene made possible by the structural changes in the reactive moiety between its ground and transition states. On the other hand, the restoring forces in the transition states of cyclobutene ring opening in *Z*-macrocycles and of thiol/disulfide exchange in both isomers were similar to those of the reactants, as in these cases the formation of the transition state did not change the molecular geometry of stiff stilbene.

The total restoring force that can be generated by stiff stilbene is probably limited to ~600 pN by the strong force dependence of the quantum yield of its $Z \rightarrow E$ photoisomerization, which decreased from ~50 % in weakly strained macrocycle **7** to <0.1 % for the generation of the highly strained *E*-isomer of **15** [25,26].

Force/rate relationship

The chemomechanical data for the two reactions is summarized in Fig. 8. In both cases, the $\ln(k_E/k_Z)_{298\ K}$ values correlate linearly with the ensemble-averaged restoring force in the reactive moiety, which indicates that the first-order (linear) Taylor expansion is sufficient to account for strain-induced variation in the rates of these two reactions up to ~500 pN [26,27]. More importantly, the slopes of both correlations (normalized to thermal energy, k_BT) equaled the ensemble-average elongation of the C1···C2 distance (Fig. 9) of both reactive moieties between their ground- and transition-state geometries (0.85 and 0.08 Å). These values are comparable to those in free reactive groups and are consistent with the mechanisms of these reactions, as described below.

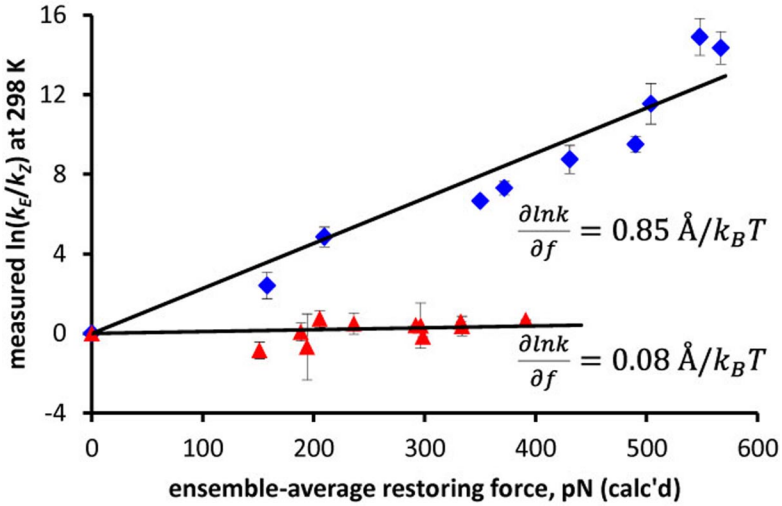

Fig. 8 Chemomechanical data acquired with molecular force probe for scissions of the C–C (diamonds) and the S–S (triangles) bonds [26,27]. Solid lines are predicted rate enhancements based on the linear (first-order) Taylor expansion using the change in the elongation of the C1···C2 distance (see below) as the value of the linear Taylor coefficient.

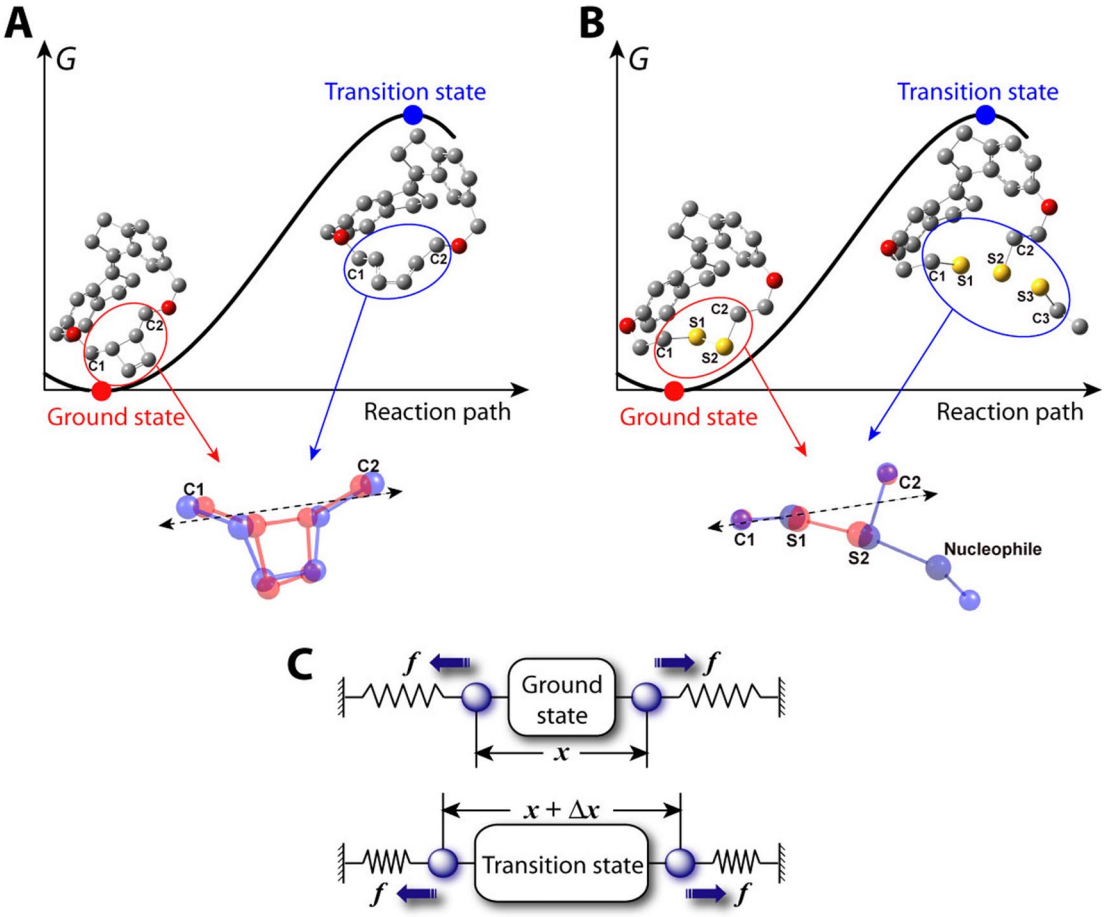

Fig. 9 Restoring force affects rates of those reactions in which nuclear motion that forms the transition state is transmitted to the rest of the system. When this net motion occurs along the restoring force vector—which is the gradient of strain energy with respect to changes in molecular geometry—a fraction of molecular strain is relieved, stabilizing the transition state. This situation occurs in the C–C bond scission in cyclobutene (A) [26], as illustrated by the overlay of the reactive moiety in its ground (red) and transition states (blue), calculated at the O3LYP/6-311+G(2d,p) level of DFT; the direction of the restoring force is shown by the broken arrow. In contrast, changes in the bond angles at S2 in S–S bond scission prevent the outward motion of the S1/S2 atoms from being transmitted to the rest of the molecule (B) [27]. (C) Generally, the simplest form of the Taylor expansion (eq. 2) would be adequate when force-dependent kinetics is driven by the relaxation of strain in the nonreactive degrees of freedom, represented here by stretched springs.

The importance of this equality is threefold. First, it allows an accurate estimate of the rate of these chemical reactions in strained molecules of any size from the knowledge of only its restoring force. On the other hand, within the formalism of strain energy, a much more detailed information about molecular structure is required to make similar predictions. Second, the equality shows that eq. 1 for these reactions is convergent, i.e., the higher-order terms make increasingly small contributions to the rate constant; for these reactions, the quadratic terms quantify the Hammond effects (strain-induced distortions of the transition and ground states). The relative contribution of the linear and quadratic terms is proportional to the stiffness of the reactive moiety and the rest of the molecule. The larger the molecule relative to the reactive moiety, the more compliant it is and hence the larger fraction of k_f arises from its relaxation, which is quantified by the linear term. Localized covalent bond rearrangements in

polymers should be particularly close to the limit of the dominant linear term, whereas strain-induced unfolding of biopolymers is probably closer to the other limit. Indeed, even in fairly small highly strained macrocycles **13–15**, the quadratic terms contribute <20 % of the observed barrier lowering (see below). Finally, the equality provides the first direct experimental evidence that an empirical coefficient in the standard chemomechanical equation (eq. 2) has a clear molecular structural meaning. In other words, within the chemomechanical formalism, the complex nuclear motion that transforms the reactant into the transition state can be quantified by changes in a single internuclear distance.

The linear term underestimates the k_f values in the smallest macrocycles **13–15** (Fig. 9) by a statistically significant amount. The additional acceleration is a manifestation of the Hammond effect, which can either decrease or increase the rate. The Hammond postulate demands that a barrier-lowering perturbation distort the reactant and the transition state toward a common geometry, thus decreasing the $f\frac{\partial \ln k}{\partial f}$ term in eq. 1 (Fig. 2), and hence k_f. Physically, the decrease reflects a less significant relaxation of the molecular force probe between the ground- and transition-state geometries of the reactive moiety as these geometries become more similar. Indeed, across the series of *E*-isomers of macrocycles **7–15**, the elongation of the C1···C2 distance from the ground to the transition state decreases by 0.25 ± 0.09 Å/nN, corresponding to a negative contribution to the quadratic term or equivalently the first-order Taylor expansion overestimating k_f values for the highest forces, opposite to what is observed.

However, distortions of the reactive moiety may also alter its intrinsic reactivity, for example, by decreasing the highest occupied molecular orbital–lowest unoccupied molecular orbital (HOMO–LUMO) gap. Such strain-induced rate perturbation is independent of the conformational relaxation of the rest of the molecule between the ground and transition states. In the case of C–C bond dissociation, the negative contribution due to the Hammond effect is more than compensated by distortions of the dihedral angles between the C_4 core and the linkers [26], which increases the reactivity of cyclobutene and contributes ~1.5 Å/nN to the quadratic term. This contribution results from ~10 % of the restoring force being orthogonal to the C1···C2 axis (Fig. 7B).

The seemingly counterintuitive difference in the kinetic responses of the C–C and S–S bond dissociations two reactions to restoring force can be readily understood by considering how the nuclear motion that transforms the reactive moieties into the respective transition states is transmitted to the motion of other nuclei of the macrocycles (Fig. 9). In the chemomechanical formalism force describes the energetic consequence of coupling of nuclear motion that constitutes a chemical reaction to motion of the rest of the system. In macrocycles **7–26**, the rest of the system is stiff stilbene and its linkers. During the C–C bond scission in cyclobutene, the two carbon atoms bound by the scissile bond move apart (by ~0.45 Å in the transition state). Because of the changes in bond angles around these atoms, the C1/C2 atoms, which connect the reactive moiety to the rest of the system, experience a larger magnitude motion (~0.85 Å). This motion occurs largely along the vector of the restoring force of the rest of the macrocycle, which by definition is the gradient of strain energy with respect to changes in geometry. It leads to a partial relief of molecular strain, which stabilizes the transition state and hence leads to the observed rate enhancements.

The formation of the transition state in thiol/disulfide exchange is also accompanied by an outward movement of the two S atoms bound by the scissile bond (Fig. 9), but this motion is not transmitted to the rest of the macrocycle. The reason again is the change in the bond angles around the electrophilic S2 atom. In both cyclobutene and disulfide, the initial angles at the scissile bonds are 107–105º; they *increase* to ~118º in the transition state of cyclobutene ring opening but *decrease* to 90º in thiol/disulfide exchange. Such a decrease is fully consistent with the established S_N2 mechanism of thiol/disulfide exchange, with its pseudo-trigonal bipyramidal transition state. The formation of this structure requires that the C2 atom (Fig. 9), which connects the electrophilic S2 atom to the rest of the macrocycle, move into the equatorial plane toward C1. Thus, the relative motion within the S1/S2 and C1/C2 atom pairs occurs in the opposite direction, negating each other. The S_N2 mechanism of

thiol/disulfide exchange uncouples the elongation of the S–S bond from the rest of the molecule. Consequently, thiol/disulfide exchange is intrinsically insensitive to restoring force along the scissile bond. This conclusion may appear counterintuitive based on our experiences from the macroscopic world, but is fully consistent with the observations of others that thiol/disulfide exchange kinetics is remarkably insensitive to molecular strain of the disulfide [55,56].

It has been often assumed that generating a restoring force along a scissile bond would always accelerate its dissociation, because the atoms bound by the scissile bond would move apart along the force vector resulting in partial relief of molecular strain. As appealing as this notion might be, the reality is more complex. Such an oversimplification neglects the fact that the energy penalty of elongating a dissociating bond can often be minimized by adjusting other bonding parameters of the atoms near the scissile bond, particularly bond angles. If such changes in bond angles decouple the elongation of the scissile bond from nuclear motion elsewhere in the molecule, no mechanism exists to lower the strain in the transition state. Nonetheless, it appears that a single internuclear distance can be found that captures the complexity of geometrical changes during the chemical reaction. This preserves the intuitively appealing notion that changes in the activation energies with restoring forces are determined by changes in the "length" of the reactive moiety along the force vector (Fig. 9C).

CONCLUSIONS AND OUTLOOK

Multiscale phenomena, lying at the interface of chemistry, materials science, nanoscience, and biology, offer complexity that will continue to intrigue and challenge chemists for decades to come. Chemomechanical approaches based on the concept of molecular restoring force hold promise for gaining a truly molecular understanding of energy flows across multiple length scales resulting from coupled motion of atoms, molecules, and macroscopic objects. They also offer the potential for exploiting such understanding for efficient design of new functional materials and for control of directional translation at the nanoscale.

Realization of this potential requires a general, quantitative, and predictive framework to relate molecular restoring forces to changes in reaction rates. Localized covalent bond rearrangements constitute the most conceptually tractable systems to develop this framework. Yet, their systematic studies are particularly challenging using the microscopic force probes that have been the standard method for controlling molecular restoring forces. A molecular force probe eliminates many constraints of its microscopic counterparts, thus greatly facilitating the acquisition and interpretation of kinetics of localized chemical reactions as a function of the restoring forces. Here we illustrated the potential of the molecular-force-probe approach by describing how it allowed us to validate experimentally the most widely used chemomechanical model (eq. 2) for the first time, to evaluate its predictive capabilities, to understand the molecular basis that govern how rates and forces are related, and to discover the unanticipated richness of such rate/force correlations.

Molecular understanding of the relationship between molecular restoring forces and chemical reactivity is still in its infancy. It seems likely that useful generalization will emerge as the technique of molecular force probe described here is applied to structurally diverse reactants and mechanistically diverse reactions, and broad comparisons are drawn both within such studies and with results of other forms of force spectroscopy, computations, and classical studies of strained molecules. The two reactions discussed here represent two major classes of reaction mechanisms, increasing our confidence that the chemomechanical formalism will be valuable in gaining deeper understating of chemical reactivity both in multiscale phenomena and in small molecules. Ultimately, chemical intuition would develop to make the concept of molecular restoring force a valuable guide to discover new chemical reactivity.

Our results show that even the simplest chemical reactions—dissociation of single covalent bonds—respond to force in ways that are more complex than could be guessed from macroscopic experience. We suggest that molecules could be designed to fragment along an axis orthogonal to their restoring force and to become more stable toward dissociation in response to stretching force. Reactions

that proceed through pre-equilibria prior to the rate-determining step would likely manifest much more complex force-rate dependences than predicted by eq. 1, as different intermediates and transition states should in general be stabilized or destabilized by restoring force to different degrees.

To date, studies of chemomechanical kinetics have focused on thermal reactions, whereas the largely unexplored photochemical kinetics in the presence of restoring force probably plays a critical role in governing the behavior of photoactuating polymers and certain molecular devices [14,45]. The approach we described above is well suited for measuring the quantum yields of diverse photochemical processes as a function of the restoring force. Yet, molecular interpretation of such data will be far more challenging since quantum-chemical calculations of conical intersections and other dynamic bottlenecks on electronically excited surfaces are much more problematic that those of stationary points in thermal processes.

Finally, chemomechanics holds great potential in guiding the design of new stress-responsive materials, including self-assessing and -healing polymers, and artificial muscles. Using the approach of molecular force probe, it is now possible to design libraries of monomers whose reactivity in stressed polymers could be predicted with useful accuracy before the polymer is synthesized and its mechanical properties are studied. This capability should allow a polymer chemist to select monomers whose strain-induced reactivity would best match that necessary to yield polymers with desired responses to bulk stresses.

ACKNOWLEDGMENTS

We are grateful to Timothy J. Kucharski, Qing-Zheng Yang, Daria Khvostichenko, and Yancong Tian who also carried out and intellectually contributed to the research described herein. The work was supported by the National Science Foundation (NSF) CAREER Award (CHE-0748281), the U.S. Air Force Office of the Scientific Research Young Investigator Award (FA9550-08-1-0072), the American Chemical Society Petroleum Research Fund (48454-AC3 and 43354-G3), and the University of Illinois. Grants of computational time were provided by the Air Force Research Lab Major Shared Resource Center and the National Center for Supercomputing Applications.

REFERENCES

1. M. M. Caruso, D. A. Davis, Q. Shen, S. A. Odom, N. R. Sottos, S. R. White, J. S. Moore. *Chem. Rev*. **109**, 5755 (2009).
2. R. Eelkema, M. M. Pollard, J. Vicario, N. Katsonis, B. S. Ramon, C. W. M. Bastiaansen, D. J. Broer, B. L. Feringa. *Nature* **440**, 163 (2006).
3. W. R. Browne, B. L. Feringa. *Nat. Nanotechnol*. **1**, 25 (2006).
4. M. Schliwa (Ed.). *Molecular Motors*, Wiley-VCH, New York (2003).
5. B. Rickborn. In *Organic Reactions*, L. A. Paquette (Ed.), p. 1, John Wiley, New York (1998).
6. M. K. Beyer, H. Clausen-Schaumann. *Chem. Rev.* **105**, 2921 (2005).
7. W. Kauzmann, H. Eyring. *J. Am. Chem. Soc*. **62**, 3113 (1940).
8. R. S. Berry, S. A. Rice, J. Ross. *Physical and Chemical Kinetics*, Oxford University Press, New York (2002).
9. J. Kopeček, J. Yang. *Polym. Int*. **56**, 1078 (2007).
10. Z. V. Todres. *Organic Mechanochemistry and its Practical Applications*, CRC Press, Boca Raton (2006).
11. S. S. Sheiko, F. C. Sun, A. Randall, D. Shirvanyants, M. Rubinstein, H.-i. Lee, K. Matyjaszewski. *Nature* **440**, 191 (2006).
12. F. H. Silver, L. M. Siperko. *Crit. Rev. Biomed. Eng*. **31**, 255 (2003).
13. K. C. Neuman, A. Nagy. *Nat. Meth*. **5**, 491 (2008).
14. T. Hugel, N. B. Holland, A. Cattani, L. Moroder, M. Seitz, H. E. Gaub. *Science* **296**, 1103 (2002).

15. D. A. Davis, A. Hamilton, J. Yang, L. D. Cremar, D. V. Gough, S. L. Potisek, M. T. Ong, P. V. Braun, T. J. Martínez, S. R. White, J. S. Moore, N. R. Sottos. *Nature* **459**, 68 (2009).
16. A. Piermattei, S. Karthikeyan, R. P. Sijbesma. *Nat. Chem*. **1**, 133 (2009).
17. C. Hyeon, D. Thirumalai. *J. Phys.: Condens. Matter* **19**, 113101 (2007).
18. C. Bustamante, Y. R. Chemla, N. R. Forde, D. Izhaky. *Annu. Rev. Biochem*. **73**, 705 (2004).
19. C. R. Hickenboth, J. S. Moore, S. R. White, N. R. Sottos, J. Baudry, S. R. Wilson. *Nature* **446**, 423 (2007).
20. S. R. White, N. R. Sottos, P. H. Geubelle, J. S. Moore, M. R. Kessler, S. R. Sriram, E. N. Brown, S. Viswanathan. *Nature* **409**, 794 (2001).
21. R. Eelkema, M. M. Pollard, N. Katsonis, J. Vicario, D. J. Broer, B. L. Feringa. *J. Am. Chem. Soc*. **128**, 14397 (2006).
22. A. Bosco, M. G. M. Jongejan, R. Eelkema, N. Katsonis, E. Lacaze, A. Ferrarini, B. L. Feringa. *J. Am. Chem. Soc*. **130**, 14615 (2008).
23. S. R. White, M. M. Caruso, J. S. Moore. *MRS Bull.* **33**, 766 (2008).
24. E. R. Kay, D. A. Leigh, F. Zerbetto. *Angew. Chem., Int. Ed*. **46**, 72 (2007).
25. Z. Huang, Q.-Z. Yang, D. Khvostichenko, T. J. Kucharski, J. Chen, R. Boulatov. *J. Am. Chem. Soc.* **131**, 1407 (2009).
26. Q.-Z. Yang, Z. Huang, T. J. Kucharski, D. Khvostichenko, J. Chen, R. Boulatov. *Nat. Nanotechnol.* **4**, 302 (2009).
27. T. J. Kucharski, Z. Huang, Q.-Z. Yang, Y. Tian, N. C. Rubin, C. D. Concepcion, R. Boulatov. *Angew. Chem., Int. Ed*. **48**, 7040 (2009).
28. P. Reimann. *Phys. Rep*. **361**, 57 (2002).
29. J. J. de Pablo, W. A. Curtin. *MRS Bull.* **32**, 905 (2007).
30. D. Cremer, E. Kraka. In *Molecular Structure and Energetics*, J. F. Liebman, A. Greenberg, (Eds.), pp. 65–138, VCH, New York (1988).
31. J. E. Leffler, E. Grunwald. *Rates and Equilibria of Organic Reactions*, Dover Publications (1989).
32. J. M. Baskin, J. A. Prescher, S. T. Laughlin, N. J. Agard, P. V. Chang, I. A. Miller, A. Lo, J. A. Codelli, C. R. Bertozzi. *Proc. Natl. Acad. Sci. USA* **104**, 16793 (2007).
33. E. Funk, F. Achenbach, J. Weis, C. Brauchle, J. Michaelis. *Langmuir* **24**, 1343 (2007).
34. P. Hanggi, F. Marchesoni. *Rev. Mod. Phys*. **81**, 387 (2009).
35. G. Hummer, A. Szabo. *Acc. Chem. Res*. **38**, 504 (2005).
36. L. B. Freund. *Proc. Natl. Acad. Sci. USA* **106**, 8818 (2009).
37. M. T. Ong, J. Leiding, H. Tao, A. M. Virshup, T. J. Martinez. *J. Am. Chem. Soc*. **131**, 6377 (2009).
38. R.-A. Jordi, S. Motoyuki, M. Dominik. *Angew. Chem., Int. Ed*. **48**, 4190 (2009).
39. J. Liang, J. M. Fernandez. *ACS Nano* **3**, 1628 (2009).
40. G. I. Bell. *Science* **200**, 618 (1978).
41. E. Evans, K. Ritchie. *Biophys. J*. **72**, 1541 (1997).
42. J. M. Lenhardt, A. L. Black, S. L. Craig. *J. Am. Chem. Soc*. **131**, 10818 (2009).
43. F. R. Kersey, W. C. Yount, S. L. Craig. *J. Am. Chem. Soc*. **128**, 3886 (2006).
44. S. Garcia-Manyes, J. Liang, R. Szoszkiewicz, T.-L. Kuo, J. M. Fernandez. *Nat. Chem*. **1**, 236 (2009).
45. N. B. Holland, T. Hugel, G. Neuert, A. Cattani-Scholz, C. Renner, D. Oesterhelt, L. Moroder, M. Seitz, H. E. Gaub. *Macromolecules* **36**, 2015 (2003).
46. J. M. Lenhardt, S. L. Craig. *Nat. Nanotechnol*. **4**, 284 (2009).
47. V. Balzani, A. Credi, M. Venturi. *Molecular Devices and Machines*, Wiley-VCH, Weinheim (2008).
48. I. Agranat, M. Rabinovitz, A. Weitzen-Dagan, I. Gosnay. *J. Chem. Soc., Chem. Commun*. 732 (1972).
49. J. E. McMurry. *Chem. Rev*. **89**, 1513 (1989).
50. J. J. Gajewski. *Hydrocarbon Thermal Isomerizations*, Elsevier, Amsterdam (2004).

51. C. Li, Q. Xu. *Cell. Signalling* **19**, 881 (2007).
52. R. Singh, G. M. Whitesides. In *Supplement S: The Chemistry of Sulphur-Containing Functional Groups*, S. Patai, Z. Rappoport (Eds.), p. 633, John Wiley, New York (1993).
53. A. P. Wiita, S. R. K. Ainavarapu, H. H. Huang, J. M. Fernandez. *Proc. Natl. Acad. Sci. USA* **103**, 7222 (2006).
54. Z. Huang, Q.-Z. Yang, T. J. Kucharski, D. Khvostichenko, S. M. Wakeman, R. Boulatov. *Chem.—Eur. J.* **15**, 5212 (2009).
55. J. A. Burns, G. M. Whitesides. *J. Am. Chem. Soc*. **112**, 6296 (2002).
56. E. L. Ruggles, P. B. Deker, R. J. Hondal. *Tetrahedron* **65**, 1257 (2009).

